

Accurate transition rates for the 5p – 5s transitions in Kr I

Krzysztof Dzierżęga,^{1,2} Udo Volz,³ Gillian Nave,^{1,4} and Ulf Griesmann^{1,4}

¹*National Institute of Standards and Technology, Gaithersburg, MD 20899–8421, U.S.A.*

²*Instytut Fizyki im. M. Smoluchowskiego, Uniwersytet Jagielloński, 30–059 Kraków, Poland*

³*Fachbereich Physik, Universität Kaiserslautern, D–67653 Kaiserslautern, Germany*

⁴*Harvard-Smithsonian Center for Astrophysics, Cambridge, MA 02138, U.S.A.*

Branching fractions were measured for electric dipole transitions from the 5p upper levels to the 5s levels in neutral krypton atoms. The measurements were made with a wall-stabilized electric arc and a 2m monochromator for the spectral lines in the visible, and with a hollow cathode lamp and the NIST 2m-Fourier transform spectrometer for the lines in the near infrared. A semi-empirical calculation, based on accurately known lifetimes for six upper levels, was used to calculate lifetimes for which accurate measurements do not exist. This resulted in a complete set of lifetimes for all 5p levels. Branching fractions and lifetimes were used to calculate transition rates for the 5p–5s transitions. The relative uncertainties of the transition rates range from less than 1% for the strongest lines to about 10% for the weakest lines. Our data also reveal that most of the previous measurements appear to have been affected by opacity effects in the light sources.

32.70.Cs, 32.70.Fw

1 Introduction

The transitions from the 5p levels to 5s levels in neutral Kr give rise to the most prominent lines in the Kr I emission spectrum (see Fig. 1 for a simplified energy level diagram). Lifetimes with sub-percent uncertainties for six of the ten 5p levels have recently been measured with beam-gas laser spectroscopy (BGLS) by Schmoranzler and Volz [1] and Schmitt *et al.* [2]. We will show below how the six lifetimes from BGLS can be used in an intermediate coupling calculation to predict accurately the lifetimes of those four levels that were not accessible to BGLS. The resulting complete set of lifetimes for the 5p levels inspired us to make new, accurate measurements of branching fractions for all 5p–5s transitions in Kr I to obtain electric dipole transition rates with uncertainties limited only by the accuracy of the radiometric calibration.

To date, the most extensive measurements of transition rates in Kr I were carried out by Chang, Horiguchi and Setser [3] who have measured transition rates for all 5p–5s transitions but with an accuracy of only 30%. Similar measurements were made by Fonseca and Campos [4, 5] who used a low-pressure spectral lamp as an excitation source and lifetimes measured in an electron excitation experiment for absolute measurements of transition rates. A number of other experiments used thermal plasma sources, either wall-stabilized electric arcs in the experiments by Ernst and Schulz-Gulde [6] and Brandt, Helbig and Nick [7] or a shock-tube in the experiment by Kaschek, Ernst and Böttcher [8]. These experiments depended on plasma diagnostics and the transition rates have relative uncertainties that are generally not much better than $\pm 10\%$ even for strong transitions.

2 Upper level lifetimes

The lifetimes of six of the ten 5p upper levels are known with relative standard uncertainties of the order of 0.2% or better from recent beam-gas-laser spectroscopy (BGLS) measurements by Schmitt *et al.* [2]. Our primary purpose here is to find reliable estimates for the lifetimes of the remaining four 5p levels. We will do this with a semi-empirical theoretical approach that is based upon intermediate coupling theory. In addition, we have evaluated the published experimental data to have an alternate set of lifetimes. Although these lifetimes are less accurate than the semi-empirical ones they provide bounds for the semi-empirical lifetimes.

2.1 Experimental lifetimes

A comparison with the six reference lifetimes from BGLS [2] divides the experimental data sets from literature in two classes of different reliability. The results from experiments employing selective laser excitation [3, 13, 14] and from the only wall-stabilized arc emission experiment [6] carried out so far generally fall (with a few explainable exceptions) into a $\pm 8\%$ tolerance band around the six reference lifetimes (see Table 1). The pulsed-laser lifetime measurements encountered some problems for the closely-spaced levels $2p_8$ and $2p_9$ due to fast collisional mixing that resulted in non-exponential decay curves. Apart from these two levels the results agree within $\pm 8\%$ with the BGLS lifetimes. A tendency towards underestimated error bars, however, is obvious for all three experiments. The lifetimes resulting from the arc emission experiment [6] also agree within $\pm 8\%$ with the BGLS results despite of an uncertainty of $\pm 30\%$ the authors quote for their absolute intensity scale. The exception here is the level $2p_9$ for which saturation problems were not adequately treated.

These measurements (summarized in Table 1) are the best measured lifetimes for the remaining four 5p levels. The estimated relative uncertainties are around $\pm 8\%$. Other experiments which employed pulsed electron excitation [15, 16, 5] or the Hanle effect [17, 18, 19, 20] all have produced at least one result far outside of the $\pm 8\%$ tolerance range and will therefore not be considered further.

2.2 Semi-empirical lifetimes

The 5p levels in krypton decay exclusively (apart from some very weak far-IR channels for the four highest 5p levels) through the transitions of the 5p–5s array. In a typical semi-empirical calculation for this transition array (e.g. Lilly [21], see column CA in Table 2) the wavefunctions of the initial and final configurations $\gamma = 4p^5 5p$ and $\gamma' = 4p^5 5s$ in intermediate coupling are expressed in terms of LS-coupled wavefunctions $|\gamma LSJM\rangle$:

$$|i, JM\rangle = \sum_{LS} |\gamma LSJM\rangle a(\gamma LSJ, i) \quad (1)$$

$$|f, J'M'\rangle = \sum_{L'S'} |\gamma' L'S'J'M'\rangle a(\gamma' L'S'J', f) \quad (2)$$

(i and f denote the coupled initial and final states). The mixing coefficients $a(\gamma LSJ, \cdot)$ can be determined from experimental energies with a semi-empirical fit procedure in the manner described by Lilly [21]. Once the mixing coefficients have been determined, the reduced dipole matrix elements $\langle i || D || f \rangle$, which are proportional to the transition rates A_{if} , may be expressed in terms of the reduced matrix elements in LS-coupling. The latter can be reduced further, using angular momentum theory, to

$$\langle \gamma LSJ || D || \gamma' L'S'J' \rangle = \delta_{SS'} (2J+1)^{1/2} (2J'+1)^{1/2} (-1)^{L+1+S+J'} \left\{ \begin{matrix} SLJ \\ 1J'L' \end{matrix} \right\} \langle \gamma LS || D || \gamma' L'S' \rangle . \quad (3)$$

In the single electron (or Coulomb) approximation the reduced dipole matrix element is proportional to the dipole transition moment $\sigma_{\gamma\gamma'}$:

$$\langle \gamma LS || D || \gamma' L' S' \rangle = (2L + 1)^{1/2} \sigma_{\gamma\gamma'} \quad (4)$$

where

$$\sigma_{\gamma\gamma'} = \sqrt{3} \int_0^\infty u_{5p}(r) e r u_{5s}(r) dr \quad (5)$$

and $u_{5p}(r)$, $u_{5s}(r)$ are the radial wavefunctions of the valence electron. In this simple semi-empirical model the relative transition rates, and thus the lifetime ratios, depend on the intermediate coupling coefficients $a(\gamma LSJ, \cdot)$ of the 5p and 5s configurations, and the absolute scale is given by one single transition moment $\sigma_{\gamma\gamma'}$ for the entire 5p–5s transition array.

When we use the transition moment $\sigma_{\gamma\gamma'} = 3.04$ a.u. that was obtained in the semi-empirical calculation by Lilly [21] we find that, on average, the six experimental BGLS lifetimes can be reproduced no better than within 7%. The predictions from this semi-empirical model for the remaining lifetimes are presumably not more accurate than the recommended experimental values are (see Table 1). It appears unlikely that the mixing coefficients of the 5s and 5p configurations are responsible for the lesser accuracy of the semi-empirical lifetimes since the reproduction of the experimental energies by the semi-empirical intermediate coupling method is quite good [21]. The problem is the assumption of one single transition moment $\sigma_{\gamma\gamma'}$ for the entire transition array. To refine the semi-empirical model, we assumed LS -dependent transition moments $\sigma_{\gamma\gamma'}(L, S, L', S')$ which correspond to LS -dependent radial functions $u_{5p}(LS)$ and $u_{5s}(L'S')$ in Eq. 5. These are similar to those used, for example, in Hartree-Fock calculations. We further assumed that spin-orbit interaction only results in a mixture of LS -terms but not in a modification of the radial wavefunctions. Since a calculation of these transition moments from first principles or from experimental energies would not have been accurate enough for our purposes we determined the transition moments from the six reference lifetimes from BGLS.

In total six different non-zero transition moments are needed for the description of the 5p–5s array. They correspond to the six allowed transitions in LS -coupling (see Table 3). In one case, for the transition $5p \ ^3D \rightarrow 5s \ ^3P$, the transition moment may be calculated directly from the lifetime of the level $2p_9$ since both the initial (3D_3) and the final state (3P_2) of the only decay channel are pure states in LS -coupling. Generally, the transition moments have to be determined by means of a nonlinear least-squares fit procedure that adjusts the transition moments so as to get best agreement of the calculated lifetimes with the six reference lifetimes from BGLS. The results are summarized in Table 3. The quoted standard uncertainties of the semi-empirical transition moments and lifetimes were obtained by Gaussian propagation of the uncertainties of the reference lifetimes, the uncertainties in the energy parameters (see [21]), and the uncertainties of the contributing branching ratios.

The energy matrices and the intermediate coupling coefficients of the 5p and 5s configurations (see Table 2) were recalculated from the Slater- and spin-orbit parameters (including the $\alpha L(L + 1)$ correction) given by Lilly [21]. The six reference states ($2p_{3,4,6..9}$) for which the lifetimes are known very accurately are mostly built from the four LS -terms 1P , 1D , 3P , and 3D . The four corresponding transition moments could thus be deduced with high accuracy (see Table 3). The transition moment of the transition $5p \ ^3S \rightarrow 5s \ ^3P$ was determined with a somewhat greater uncertainty from the lifetime of the $2p_3$ state. This state is the only one in the set of reference states that contains a relevant contribution (16%) from the 3S term. The 1S term only contributes to the states $2p_1$ and $2p_5$ which are not included in the set of reference states. For the determination of the transition moment of the transition $5p \ ^1S \rightarrow 5s \ ^1P$ we resorted to branching fractions as additional criteria. Particularly, we used branching fractions of the weak decay channels $2p_1 \rightarrow 1s_4$ and $2p_5 \rightarrow 1s_2$ which are sensitive to the transition moment sought after. The dependence of the branching fractions for these transitions and the upper level lifetimes on the transition moment is shown in figure Fig. 3. The attainable accuracy for the transition moment, however, is limited by the uncertainty in the branching fractions.

As a last technical detail we note that for the four highest 5p levels ($2p_1 \dots 2p_4$) there are weak far-IR decay channels to states of the 4d configuration which have to be accounted for. For this purpose we used the theoretical transition rates calculated by Aymar and Coulombe [23]. Because of the huge discrepancies between length- and velocity-form results for the 5p–4d transition rates we used the greater velocity-form results with a pessimistic uncertainty estimate of $\pm 100\%$ (see Table 2).

The uncertainties of the four semi-empirical lifetimes (see Table 2) for the states $2p_1$, $2p_2$, $2p_5$, and $2p_{10}$ vary between 0.1% and 3.7% depending on the LS -terms they are built from. The $2p_2$ state allows for a very precise lifetime calculation because it relates to the four accurately determined transition moments only. The lifetime predictions for the other three levels are less accurate because they include significant contributions from the two less accurate transition moments. Our semi-empirical predictions agree very well with the best previous experimental values (see column BE in Table 1) but they are of superior accuracy and we used them for the normalization of our transition rates.

3 Branching fractions

The measurement of branching fractions for the transition from 5p levels presents a formidable task owing to the metastable nature of the lower 5s and 5s' levels (see Fig. 1) which may render the lamp discharge column optically thick for transitions to those levels. We have measured branching fractions for 30 lines arising from 5p levels in the wavelength range from 556.2 nm to 1878.5 nm in two separate experiments. The spectral lines in the visible part of the Kr I spectrum were measured in air with a wall-stabilized arc discharge and a 2m – Czerny-Turner monochromator. The infrared portion of the spectrum was measured with a hollow-cathode lamp and the NIST 2m – Fourier transform spectrometer. The comparison of the results from the two different experiments made it easier for us to notice systematic errors due to optically thick transitions in the light sources. The four $5p' - 4d$ transitions (see Fig. 1) near 10000 nm were outside the range of either experiment.

3.1 Wall-stabilized arc measurements

The experimental setup for the measurements is shown schematically in Fig. 2. In our experiment we used the wall-stabilized arc previously described in detail by Musielok *et al.* [9]. The space near the electrodes was operated in argon while the midsection of the arc channel contained helium with a small admixture of krypton. The fraction of krypton in helium was maintained below 0.3% to avoid self-absorption of krypton lines. The arc was operated at a current of 50 A. To check for optical thickness, the krypton spectra were measured with varying amounts of krypton in the discharge.

When the wall-stabilized arc is operated in helium, spectral lines remain narrow and continuum emission is low because of the low electron density in a helium arc. This facilitates more accurate line intensity measurements because spectral lines are well isolated and the ratio of line to continuum intensity is high. It was not necessary to achieve LTE conditions in the arc plasma, because we were only interested in the measurement of branching ratios of spectral lines. The measurements were performed in a side-on configuration to avoid interloping argon lines and argon plasma continuum radiation that are emitted at the ends of the arc. As indicated in Fig. 2, either the wall-stabilized arc or a tungsten strip standard lamp were imaged onto the entrance slit of a 2 m Czerny–Turner monochromator by a concave mirror with a magnification factor of approximately 1.3. A beam splitter was placed in the beam path to reflect a fraction of the light into the 0.25 m monochromator that was used to monitor the discharge stability. This monochromator was set to the 760.2 nm line of Kr I. The total intensity of this line was measured with a photomultiplier tube and a chart recorder and showed less than 1% fluctuation during our measurements. The krypton spectra were recorded with a CCD camera that was mounted at the exit plane of the monochromator. The measured spectral line profiles were first corrected for the spectral response of the experimental system, as determined with the standard lamp, and the residual continuum was subtracted. The lines were then

integrated by fitting a spline function to the data using a program package published by Renka[10] which yields the integral of the spectral line without requiring that the apparatus function be known analytically.

3.2 Hollow cathode lamp measurements

The experiment described in the previous section was unsuited for measurements in the infrared because it was set up in air. A second experiment in a purged environment was therefore carried out to measure the intensity of lines in the infrared. This used a high-resolution Fourier transform spectrometer to observe spectra of a hollow cathode lamp.

The high-current hollow cathode lamp we used was developed by Danzmann *et al.* [11]. For our measurements it was equipped with a cathode made of oxygen-free copper which is easy to operate and has no lines that blend with the krypton lines of interest. The hollow cathode lamp was operated with between 130 Pa and 250 Pa of argon or neon as a carrier gas for the discharge with an admixture of between 0.5 Pa and 10 Pa. The discharge current was varied between 100 mA and 500 mA. The experimental setup was similar to the one used with the wall-stabilized arc. The entire imaging system was enclosed in a purge box that was continuously purged with water vapor and carbon dioxide free air to suppress absorption by these gases in the near infrared.

Many lines were strongly self-absorbed when pure krypton was used as a carrier gas in the hollow cathode lamp discharge. This problem was partly overcome when the partial pressure of krypton in the discharge was reduced by using a neon-krypton mixture in the hollow cathode lamp. We also found that the spectra obtained with high currents where the copper density in the discharge is high show self absorption only in the very strongest lines. We assume that the metastable 5s states were depopulated by charge-transfer collisions with copper atoms in the hollow cathode lamp discharge.

The NIST 2m – Fourier transform spectrometer (described in Nave *et al.* [12]) was used to measure the spectra of the hollow cathode lamp and the standard lamp. A resolution of around 0.01 cm^{-1} was used for the measurements of the krypton spectra. For the near IR region, a liquid nitrogen cooled indium-antimonide detector was used whereas silicon photodiodes were used to record spectra below 1000 nm. To improve the signal-to-noise ratio, colored glass filters were employed to restrict the bandpass of the spectrometer to the wavenumber range of interest. The spectral sensitivity of the optical and detection systems was calibrated with the standard lamp before and after measurements of the spectra of the light from the hollow cathode discharge. Some residual self-absorption was evident for the strongest lines even at low krypton partial pressures. For those lines we relied on the results from the experiment with the wall-stabilized arc, where these lines remained optically thin.

3.3 Data analysis and uncertainties

It is common that the the uncertainty of experimental transition rates is limited by the uncertainty of the measurement of the upper level lifetimes and not by the uncertainty of the branching fraction measurement. In our case, the situation is reversed. The uncertainty of the branching fraction measurement is limited by the uncertainty of the radiometric calibration which is around 2%. The uncertainties of the upper level lifetimes are generally much lower. In this section we will describe in detail how the uncertainties for the branching fractions were calculated.

The transition rate A_{ki} of a transition from a particular upper level k to lower level i can be calculated from a measurement of the upper level lifetime τ_k and a measurement of the branching fraction F_{ki} – the fraction that the transition to i contributes to the total decay rate:

$$A_{ki} = \frac{1}{\tau_k} F_{ki}, \quad \text{where} \quad F_{ki} = \frac{A_{ki}}{\sum_j A_{kj}}. \quad (6)$$

The branching fractions can in turn be calculated from the relative intensities I_{ki} of the lines (in photons/s)

by

$$F_{ki} = \frac{I_{ki}}{\sum_j I_{ki}} \quad (7)$$

where the sum is over all the lower levels to which the upper level can decay.

Several independent measurements of the Kr I spectrum were made with different operating conditions for the hollow cathode lamp. The relative intensity \hat{I}_{ki}^α of each spectral line in each measured spectrum α was calculated from the observed intensity I_{ki}^α and the relative efficiency of the spectrometer $\epsilon(\sigma)$ at the wavenumber σ of the spectral line by:

$$\hat{I}_{ki}^\alpha = \frac{I_{ki}^\alpha(\sigma)}{\epsilon(\sigma)} \quad (8)$$

where the relative efficiency of the optical system was assumed to be constant over the width of the spectral line. These intensities were then divided by a normalizing factor $\hat{I}_{\text{norm}}^\alpha$ to put all the intensities in all spectra on the same relative intensity scale. This normalizing factor was usually chosen such that the intensity of one strong line common to all spectra was 1, hence making the intensities relative with respect to that strong line. This approach was found to be more reliable than using a weighted mean of the intensities, as lines in some of the spectra may be affected by self-absorption, or be too weak to be measured. The weighted mean relative intensity of the line \bar{I}_{ki} was then found using:

$$\bar{I}_{ki} = \frac{1}{\sum_\alpha w_{ki}^\alpha} \sum_\alpha \frac{w_{ki}^\alpha \hat{I}_{ki}^\alpha}{\hat{I}_{\text{norm}}^\alpha} \quad (9)$$

where w_{ki}^α is a weighting factor. The weighting factor chosen for the hollow cathode measurements was the signal-to-noise ratio of the line. The small uncertainty of the normalization line intensity is due to its high signal-to-noise ratio. These branching ratios are converted to branching fractions and transition rates using equations 6 and 7.

Absolute transition rates are then determined from the mean values of between 5 and 9 independent measurements of the relative intensities and experimental lifetime data. They are presented in table 4, along with the lifetimes of the upper levels used to determine the transition rates. The uncertainties given in the table result from the estimated standard deviation of the branching fractions and the uncertainty of the lifetime data. The estimated standard deviation of the branching fractions depends on the uncertainty in the weighted mean relative intensity, which in turn depends on the individual measurements of the intensity through equation 9, and the uncertainty in the radiometric calibration of the spectrometer.

The estimated uncertainty in the individual measurements of the intensity was taken as the intensity divided by the signal-to-noise ratio: $\hat{I}_{ki}^\alpha/w_{ki}^\alpha$. When photon noise is the dominant source of uncertainty, the square of the signal-to-noise ratio must be used as the weighting factor in equation 9. We chose to weight the individual intensity measurements with the signal-to-noise ratio to account for a significant systematic component in the uncertainty which may result from self-absorption or line blends.

The statistical component in the uncertainty of the weighted mean relative intensity $u_{\text{stat}}(\hat{I}_{ki})$ can then be derived by applying the law of propagation of uncertainty to equation 9:

$$u_{\text{stat}}(\bar{I}_{ki}) = \sqrt{\sum_\alpha \left(\frac{\hat{I}_{ki}^\alpha}{\hat{I}_{\text{norm}}^\alpha} \cdot \frac{1}{w_{ki}^\alpha} \right)^2}$$

where the sum is again over all the observations of the lines. This must be added in quadrature to the uncertainty in the radiometric calibration of the spectrometer, which was estimated at 3.3% for one standard deviation. This estimate includes the uncertainty in the supplied calibration of the standard lamp (1.5% for one standard deviation) and a contribution of 3% for the measurement of the standard lamp spectrum. The total uncertainty in the measurement of the weighted mean relative intensities is thus:

$$u(\bar{I}_{ki}) = \sqrt{u_{\text{stat}}^2(\bar{I}_{ki}) + (0.033\bar{I}_{ki})^2} \quad (10)$$

The uncertainty in the measurement of the branching fractions $u(F_{ki})$ is derived by applying the law of propagation of uncertainty to equation 7 to give:

$$u(F_{ki}) = \sqrt{\frac{u^2(\bar{I}_{ki})}{(\sum_i \bar{I}_{ki})^2} + \frac{\bar{I}_{ki}^2}{(\sum_i \bar{I}_{ki})^4} \sum_j u^2(\bar{I}_{ki})} \quad (11)$$

This is combined in quadrature with the uncertainty in the lifetime $u(\tau_k)$ to give the uncertainty in the transition rate $u(A_{ki})$:

$$u(A_{ki}) = \sqrt{\frac{1}{\tau_k^2} u^2(F_{ki}) + \frac{F_{ki}^2}{\tau_k^4} u^2(\tau_k)} \quad (12)$$

For the wall-stabilized arc measurements, the transition rates and their uncertainties were calculated similarly.

4 Discussion of results

Our new transition rates for 5p – 5s transitions in Kr I are listed in Table 4. Also listed in Table 4 are our experimental branching fractions and the lifetimes that were used to calculate the transition rates.

In Table 5 and Fig. 4 we compare our transition rates with several experimental results. The only other measurement that includes the lines in the IR is that of Chang, Horiguchi and Setser [3] and a comparison of those results with our data is shown in Fig. 5. The results by Fonseca and Campos [4, 5], presented in Fig. 4, were recalculated using the same lifetime data as in our work. For the set of strong lines around 800 nm our transition rates are in good agreement with most of the results obtained by Fonseca and Campos [4, 5] and differ from those obtained by Ernst *et al.* [6] by about 10%. The results of Kaschek *et al.* [8] differ from ours by a constant scaling factor of 1.3, on average. Only in the case of the line at 810.4 nm, all other experimental data exceed our result by 20%–30%.

The most striking difference between previous measurements and our results is that our transition rates for the set of weak lines near 600 nm are much lower than all previous measurements with the exception of the experiment by Brandt, Helbig and Nick [7]. This strongly suggests that many of the earlier experiments had problems with self-absorption of the strong lines around 800 nm which would make the weak lines in a set of transitions from a particular upper level appear stronger.

It is also interesting to compare our results with the theoretical calculations because all calculations were intermediate-coupling calculations in the Coulomb approximations whereas our semi-empirical lifetimes were obtained with a modified intermediate-coupling scheme. Fig. 6 compares our results to the most recent calculations. The earlier calculations by Murphy [22] are not included because they were superseded by those of Lilly [21]. For the strongest lines near 800 nm the best agreement, within 10% on average, was found between our data and calculations made by Aymar and Coulombe [23] with a velocity dipole operator, while there is a constant disagreement (a factor of 1/3) when they used a length dipole operator. A similar discrepancy was found with calculations made by Lilly [21]. We note that the discrepancies for the weak lines near 600 nm and in the IR are considerable but there appear to be no conspicuous systematic trends as we found in the experimental data.

Acknowledgments

K. Dzierżęga gratefully acknowledges financial support from the Maria Skłodowska-Curie Foundation through grant number MEN–NIST–96–260. We are grateful to W. L. Wiese, NIST, K. Musioł, Jagiellonian University, Kraków, and H. Schmoranzler, University of Kaiserslautern for helpful discussions and continued support. G. Nave and U. Griesmann were supported by NIST contracts number 43SBNB867005 and 43SBNB960002 to Harvard College Observatory.

References

- [1] H. Schmoranzer and U. Volz, Phys. Scr. **T47**, 42–48 (1993).
- [2] A. Schmitt, N. Pisella, U. Volz, and H. Schmoranzer, 6th International Colloquium on Atomic Spectra and Oscillator Strengths for Astrophysical and Laboratory Plasmas (ASOS6). Abstracts of Contributed Oral Papers and Poster Papers, Ed. J. Tatum, University of Victoria (Victoria, BC), p.143 (1998).
- [3] R. S. F. Chang, H. Horiguchi, and D. W. Setser, J. Chem. Phys. **73**, 778 (1980).
- [4] V. Fonseca and J. Campos, Physica **97C**, 312 (1979).
- [5] V. Fonseca and J. Campos, J. Phys. B **13**, 3957 (1980).
- [6] W. E. Ernst and E. Schulz–Gulde, Physica **93C**, 136 (1978).
- [7] T. Brandt, V. Helbig and K.–P. Nick, J. Phys. B **15**, 2139 (1982).
- [8] K. Kaschek, G. Ernst and W. Böttcher, Physica **123C**, 238 (1984).
- [9] J. Musielok, W. L. Wiese and G. Veres, Phys. Rev. A **51**, 3588 (1995).
- [10] R. J. Renka, SIAM J. Sci. Stat. Comp. **8**, 393 (1987).
- [11] K. Danzmann, M. Günther, J. Fischer, M. Kock and M. Kühne, Appl. Opt. **27**, 4947 (1988).
- [12] G. Nave, C. J. Sansonetti and U. Griesmann, “*Progress on the NIST IR–vis–UV Fourier transform spectrometer*”, in Fourier Transform Spectroscopy, Vol. 3, 1997 OSA Technical Digest Series (Optical Society of America, Washington DC, 1997), 38 (1997).
- [13] B. D. Cannon, W. L. Glab, and R. Ogorzalek-Loo, Phys. Rev. **A47**, 147 (1993).
- [14] C. A. Whitehead, H. Pournasr, M. R. Bruce, H. Cai, J. Kohel, W. B. Layne, and J. W. Keto, J. Chem. Phys. **102**, 1965 (1995).
- [15] A. L. Osherovich and Ya. F. Verolainen, Leningrad State University Vestnik, **N4**, 140 (1967).
- [16] M. V. Fonseca and J. Campos, Phys. Rev. **A17**, 1080 (1978).
- [17] D. A. Landman and R. Dobrin, Phys. Rev. **A8**, 1868 (1973).
- [18] J.-P. Lemoigne, X. Husson, and J. Margerie, Opt. Commun. **15**, 241 (1975).
- [19] S. A. Kazantsev, A. G. Rys, and M. P. Chaika, Opt. Spectrosc. **44**, 249 (1978).
- [20] M. B. Gorny, S. A. Kazantsev, B. G. Matisov, and N. T. Polezhaevs, J. Phys. B **322**, 322 (1985).
- [21] R. A. Lilly, J. Opt. Soc. Am. **66**, 245 (1976).
- [22] P. W. Murphy, J. Opt. Soc. Am. **58**, 1200 (1968).
- [23] M. Aymar and M. Coulombe, Atomica Data and Nuclear Data Tables **21**, 537 (1978).

Table 1: Experimental lifetimes of the KrI 5p states. (Uncertainties are given in parentheses.)

Level		Experimental lifetimes (ns)					
		WSA ¹ [6]	PL ² [3]	PL ² [13, 14]	BGLS ³ [1]	BGLS ³ [2]	BE ⁴
2p ₁	5p'[1/2] ₀	24.6(1.5)	—	—	—	—	24.6(2.0)
2p ₂	5p'[3/2] ₂	32.0(1.9)	26.9(0.3)	—	—	—	29.5(2.4)
2p ₃	5p'[1/2] ₁	27.2(1.6)	26.8(1.7)	—	—	28.075(30)	
2p ₄	5p'[3/2] ₁	27.9(1.7)	27.2(1.6)	—	—	29.402(42)	
2p ₅	5p [1/2] ₀	23.4(1.4)	—	23.5(1.0) [14]	—	—	23.5(1.9)
2p ₆	5p [3/2] ₂	28.6(1.7)	25.4(0.8)	26.4(0.5) [14]	27.35(6)	27.345(16)	
2p ₇	5p [3/2] ₁	32.3(1.9)	29.7(1.0)	—	29.51(6)	29.619(17)	
2p ₈	5p [5/2] ₂	29.6(4.6)	26.5(2.0)	32.5(0.8) [13]	32.10(9)	32.041(47)	
2p ₉	5p [5/2] ₃	34.6(+2.2, -5.8)	28.7(2.0)	30.2(1.4) [13]	27.73(7)	27.694(18)	
2p ₁₀	5p [1/2] ₁	—	40.9(1.7)	—	—	—	40.9(3.3)

¹Wall-stabilized arc emission. Quoted uncertainties do not include the uncertainty of the absolute intensity scale for the transition rates of $\pm 30\%$.

²Lifetimes from pulsed laser excitation.

³Lifetimes from beam-gas-laser spectroscopy.

⁴Best estimate of non-BGLS experimental lifetimes.

Table 2: Semi-empirical lifetimes and decomposition in *LS*-terms for the KrI 5p states.

Level		<i>LS</i> decomposition ¹ (%)						Far-IR	Lifetimes (ns)	
		¹ S	¹ P	¹ D	³ S	³ P	³ D	branches ² (%)	CA ³ [21]	this work ⁴
2p ₁	5p'[1/2] ₀	43	—	—	—	57	—	0.246	24.37	24.58 \pm 0.85
2p ₂	5p'[3/2] ₂	—	—	34	—	21	44	0.034	29.10	28.59 \pm 0.07
2p ₃	5p'[1/2] ₁	—	19	—	16	61	3	0.106	26.35	28.08 \pm 0.07
2p ₄	5p'[3/2] ₁	—	24	—	1	1	74	0.0045	30.65	29.34 \pm 0.04
2p ₅	5p [1/2] ₀	57	—	—	—	43	—	—	23.54	23.12 \pm 0.85
2p ₆	5p [3/2] ₂	—	—	22	—	75	4	—	25.43	27.34 \pm 0.02
2p ₇	5p [3/2] ₁	—	53	—	—	24	23	—	30.09	29.62 \pm 0.02
2p ₈	5p [5/2] ₂	—	—	44	—	4	52	—	34.03	32.05 \pm 0.06
2p ₉	5p [5/2] ₃	—	—	—	—	—	100	—	28.77	27.70 \pm 0.02
2p ₁₀	5p [1/2] ₁	—	4	—	83	14	—	—	40.30	38.13 \pm 1.07

¹Recalculated from the parameters given by Lilly [21].

²Total far-IR (5p-4d) decay rate over total decay rate. Estimated uncertainty $\pm 100\%$.

³Intermediate coupling with transition moment from Coulomb approximation.

⁴Intermediate coupling with *LS*-dependent transition moments from Table 3. Note the excellent agreement of these semi-empirical lifetimes with the experimental BGLS lifetimes in Table 1.

Table 3: LS -dependent transition moments for the KrI 5p-5s transition array.

Transition		Transition moment σ (a.u.)
5p 1S	\longrightarrow 5s 1P	3.22 ± 0.18
5p 1P	\longrightarrow 5s 1P	3.146 ± 0.003
5p 1D	\longrightarrow 5s 1P	3.205 ± 0.014
5p 3S	\longrightarrow 5s 3P	3.173 ± 0.057
5p 3P	\longrightarrow 5s 3P	2.853 ± 0.073
5p 3D	\longrightarrow 5s 3P	3.085 ± 0.001

Table 4: Branching fractions F_{ki} and absolute transition rates A_{ki} for all 30 5p – 5s transitions in neutral Kr.

Upper level	Lower level	λ (nm)	τ (ns) ¹	F_{ki} (WSA) ²	F_{ki} (HCL) ³	A_{ki} (10 ⁶ s ⁻¹)
5p'[1/2] ₀ (2p ₁)	5s[3/2] ₁ (1s ₄)	557.31	<i>24.58±0.85</i>	<10 ⁻³		<0.04
	5s'[1/2] ₁ (1s ₂)	768.52		>0.999		40.64±0.2
5p'[3/2] ₂ (2p ₂)	5s[3/2] ₂ (1s ₅)	556.22	<i>28.59±0.07</i>	0.003±0.004		0.11±0.01
	5s[3/2] ₁ (1s ₄)	587.09		0.020±0.004		0.71±0.14
	5s'[1/2] ₁ (1s ₂)	826.32		0.977±0.005		34.16±0.19
5p'[1/2] ₁ (2p ₃)	5s[3/2] ₂ (1s ₅)	557.03	28.075±0.03	0.028±0.0016		0.98±0.056
	5s[3/2] ₁ (1s ₄)	587.99		0.002±0.0002		0.055±0.006
	5s'[1/2] ₀ (1s ₃)	785.48		0.573±0.008		20.41±0.5
	5s'[1/2] ₁ (1s ₂)	828.11		0.398±0.014		14.18±0.5
5p'[3/2] ₁ (2p ₄)	5s[3/2] ₂ (1s ₅)	567.25	29.402±0.042	0.00044±0.0001		0.015±0.003
	5s[3/2] ₁ (1s ₄)	599.39		0.0015±0.0002		0.050±0.007
	5s'[1/2] ₀ (1s ₃)	805.95		0.465±0.014		15.83±0.49
	5s'[1/2] ₁ (1s ₂)	850.89		0.533±0.015		18.11±0.51
5p[1/2] ₀ (2p ₅)	5s[3/2] ₁ (1s ₄)	758.74	<i>23.12±0.85</i>		0.9965±0.0033	43.10±0.6
	5s'[1/2] ₁ (1s ₂)	1212.35			0.0035±0.0003	0.15±0.015
5p[3/2] ₂ (2p ₆)	5s[3/2] ₂ (1s ₅)	760.15	27.345±0.016	0.743±0.007	0.751±0.008	27.32±0.18
	5s[3/2] ₁ (1s ₄)	819.01		0.248±0.009	0.241±0.008	8.94±0.22
	5s'[1/2] ₁ (1s ₂)	1373.89			0.0083±0.0003	0.31±0.01
5p[3/2] ₁ (2p ₇)	5s[3/2] ₂ (1s ₅)	769.45	29.619±0.017	0.127±0.004	0.127 ±0.004	4.27±0.11
	5s[3/2] ₁ (1s ₄)	829.81		0.868±0.005		29.31±0.18
	5s'[1/2] ₀ (1s ₃)	1286.19			0.0031±0.0002	0.076±0.005
	5s'[1/2] ₁ (1s ₂)	1404.57			0.0023±0.0001	0.106±0.006
5p[5/2] ₂ (2p ₈)	5s[3/2] ₂ (1s ₅)	810.44	32.041±0.047	0.288 ±0.015	0.287±0.009	8.96±0.29
	5s[3/2] ₁ (1s ₄)	877.68		0.709 ±0.01	0.710±0.009	22.17±0.29
	5s'[1/2] ₁ (1s ₂)	1547.40			0.0026±0.0001	0.081±0.004
5p[3/2] ₃ (2p ₉)	5s[3/2] ₂ (1s ₅)	811.29	27.694±0.018	1.00	1.00	36.1±0.09
5p[1/2] ₁ (2p ₁₀)	5s[3/2] ₂ (1s ₅)	892.87	<i>38.13±1.07</i>	0.873 ±0.004		22.89±0.65
	5s[3/2] ₁ (1s ₄)	975.18		0.120 ±0.004	0.120±0.004	3.13±0.14
	5s'[1/2] ₀ (1s ₃)	1672.65			0.0048±0.0002	0.126±0.006
	5s'[1/2] ₁ (1s ₂)	1878.55			0.0028±0.0001	0.074±0.003

¹Lifetimes of the upper levels are experimental lifetimes from Schmitt *et al.* [2] (see also Table 1) and semi-empirical lifetimes from Table 2. Semi-empirical lifetimes are printed in italics.

²Wall-stabilized arc measurement.

³Hollow-cathode lamp measurement.

Table 5: Compilation of experimental and theoretical transition rates for 5p – 5s transitions in Kr I.

Upper level	Lower level	λ (nm)	$A_{ki}(10^6 \text{ s}^{-1})$ ¹	[6]	[4, 5]	[7]	[8]	[3]	[21]	[23] ²	[23] ³
5p'[1/2] ₀	5s[3/2] ₁	557.31	<0.04		0.09			0.09	0.06	0.437	0.251
	5s'[1/2] ₁	768.52	40.64(20)	40.7	40.2			45.2	41.19	49.6	32.9
5p'[3/2] ₂	5s[3/2] ₂	556.22	0.11(1)	0.23	0.36	0.18		0.27	0.49	0.595	0.201
	5s[3/2] ₁	587.09	0.71(14)	1.48	1.8	0.86		1.6	1.92	2.39	0.933
	5s'[1/2] ₁	826.32	34.16(19)	29.5	32.8		42.8	35.3	32.31	41.1	32.2
5p'[1/2] ₁	5s[3/2] ₂	557.03	0.980(56)	1.71	2.4	1.37		1.9	3.18	3.91	1.32
	5s[3/2] ₁	587.99	0.055(6)		0.13	0.049		0.093	0.14	0.198	0.0848
	5s'[1/2] ₀	785.48	20.41(50)	19.5	20.6			21.2	20.27	25.4	18.0
	5s'[1/2] ₁	828.11	14.18(50)	15.6	13.3		19.5	14.2	14.62	18.8	14.7
5p'[3/2] ₁	5s[3/2] ₂	567.25	0.015(3)		0.02	0.022		0.02	0.01	0.00455	0.00168
	5s[3/2] ₁	599.39	0.050(7)		0.09	0.052		0.07	0.06	0.0841	0.0397
	5s'[1/2] ₀	805.95	15.83(49)	15.8	15.7		22.6	17.5	16.44	21.2	15.8
	5s'[1/2] ₁	850.89	18.11(51)	20.0	18.3			19.1	16.37	20.6	17.1
5p[1/2] ₀	5s[3/2] ₁	758.74	43.1(6)	42.8			58.2	43.8	42.8	52.4	33.8
	5s'[1/2] ₁	1212.35	0.150(15)					0.04	0.01	0.00143	0.000407
5p[3/2] ₂	5s[3/2] ₂	760.15	27.32(18)	25.8	27.3		35.6	28.6	30.28	38.6	25.5
	5s[3/2] ₁	819.01	8.94(22)	9.15	9.3		12.5	10.4	9.23	11.6	8.88
	5s'[1/2] ₁	1373.89	0.31(1)					0.3	0.13	0.164	0.356
5p[3/2] ₁	5s[3/2] ₂	769.45	4.27(11)	4.7	4.4			4.41	5.01	6.52	4.42
	5s[3/2] ₁	829.81	29.31(18)	26.3	29.5			29.0	28.40	36.0	28.3
	5s'[1/2] ₀	1286.19	0.076(5)					0.10	0.03	0.0345	0.0664
	5s][1/2] ₁	1404.57	0.106(6)					0.13	0.05	0.0633	0.141
5p[5/2] ₂	5s[3/2] ₂	810.44	8.96(29)	11.0	10.9		11.7	8.16	9.99	12.6	9.5
	5s[3/2] ₁	877.68	22.17(29)	22.8	20.2			22.9	19.59	26.1	22.2
	5s'[1/2] ₁	1547.40	0.081(4)					0.09	0.04	0.0477	0.131
5p[3/2] ₃	5s[3/2] ₂	811.29	36.10(9)	28.9			39.0	34.8	35.03	44.6	33.7
5p[1/2] ₁	5s[3/2] ₂	892.87	22.89(65)	30.7	26.2			19.8	22.30	28.4	26.1
	5s[3/2] ₁	975.18	3.13(14)		3.4			4.28	2.63	3.43	3.75
	5s'[1/2] ₀	1672.65	0.126(6)					0.15	0.05	0.0617	0.201
	5s'[1/2] ₁	1878.55	0.074(3)					0.17	0.03	0.0344	0.143

¹From Table 4

²Length form

³Velocity form

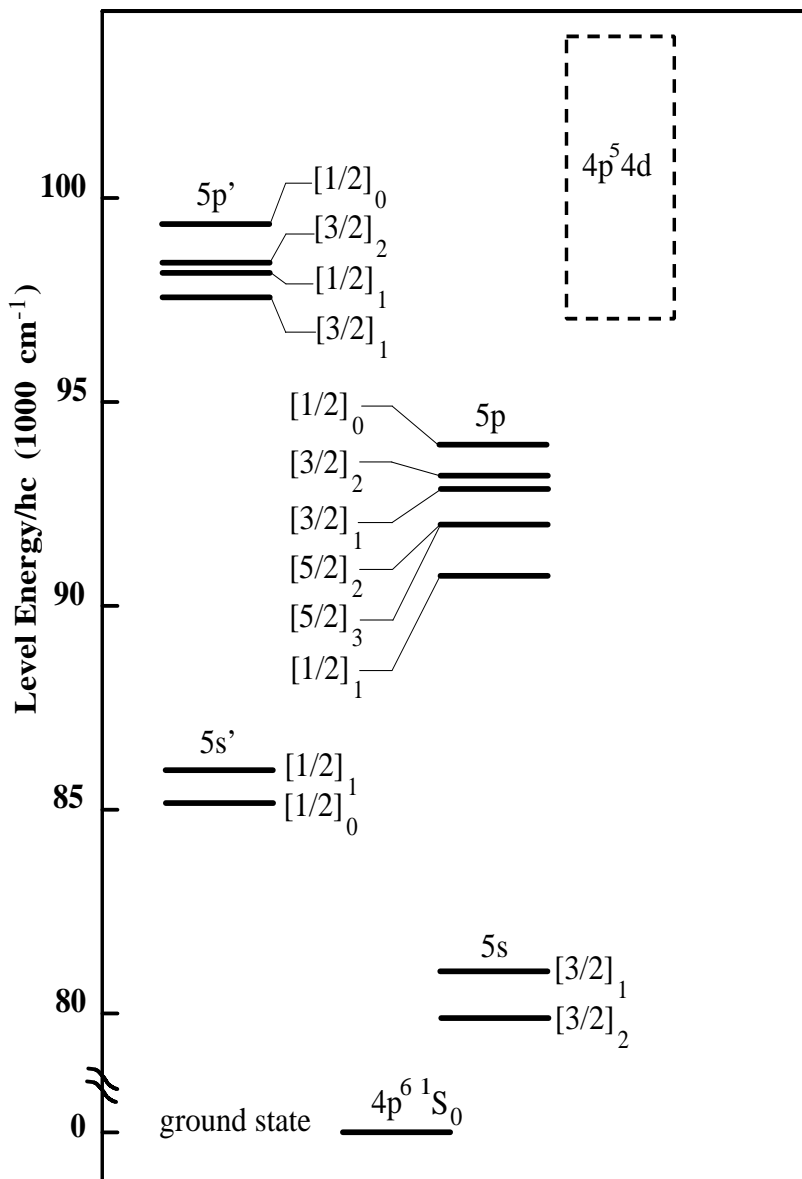


Figure 1: 5s and 5p energy levels of Kr I. The levels are labeled in $J_c K$ -coupling notation which is the most appropriate for the spectra of the noble gases. The primed and unprimed levels are distinguished by their different core angular momenta J_c . The core level of the unprimed levels is $4p^5 \ ^2P_{3/2}$ whereas it is $4p^5 \ ^2P_{1/2}$ for the primed levels. The two 5s levels with angular momenta of 0 and 2 cannot decay into the ground state via electric dipole transitions. Several transitions from 5p' levels to $4p^5 \ 4d$ levels in the infrared near 10000 nm are outside the wavelength range that was accessible in our experiments.

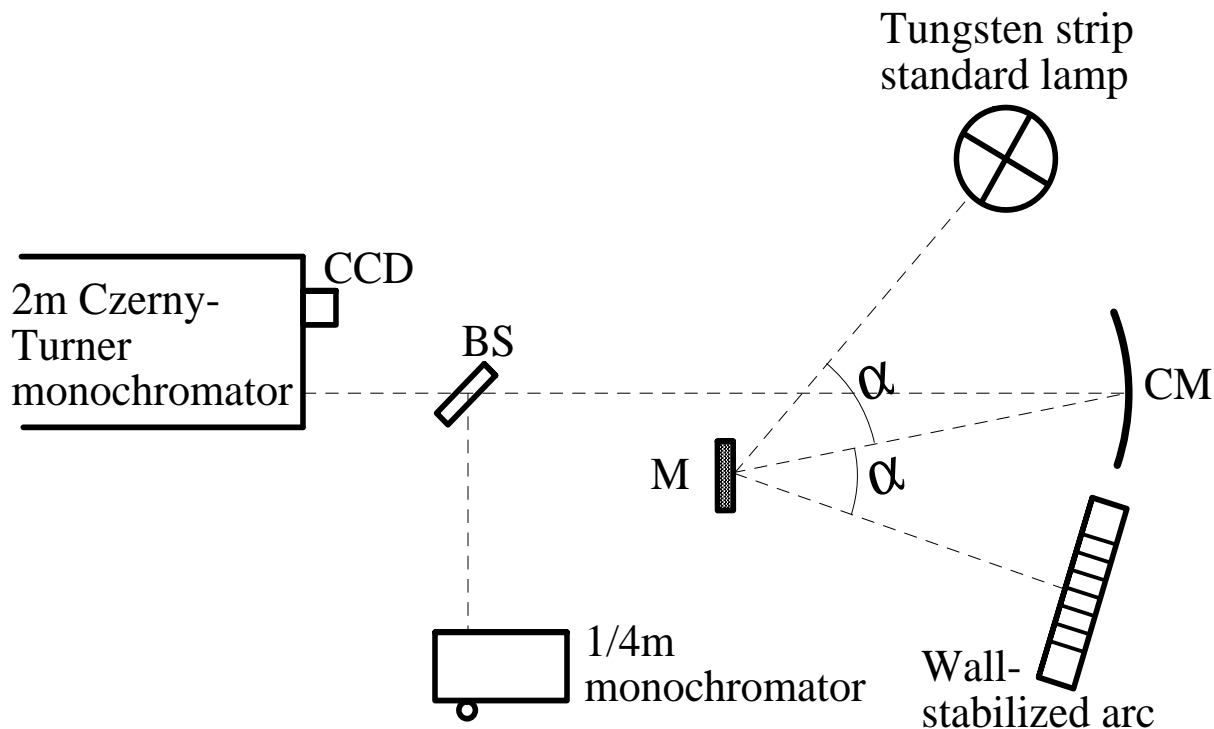


Figure 2: Schematic of the experimental setup for the measurements with the wall-stabilized arc. The radiation from the arc or the radiometric standard lamp were imaged onto the entrance slit of a 2m-monochromator by a curved mirror CM. A flat mirror M, that was mounted on a turntable allowed to alternate between both lightsources. A small fraction of the light was imaged onto the entrance slit of a 1/4m-monochromator with a beam splitter BS. This monochromator remained set to the Kr I line at 760.2 nm to monitor the stability of the arc discharge. The experimental setup for the measurements with the NIST 2m – Fourier transform spectrometer was identical but the imaging system was enclosed in a box that was purged with water vapor- and carbon dioxide- free air.

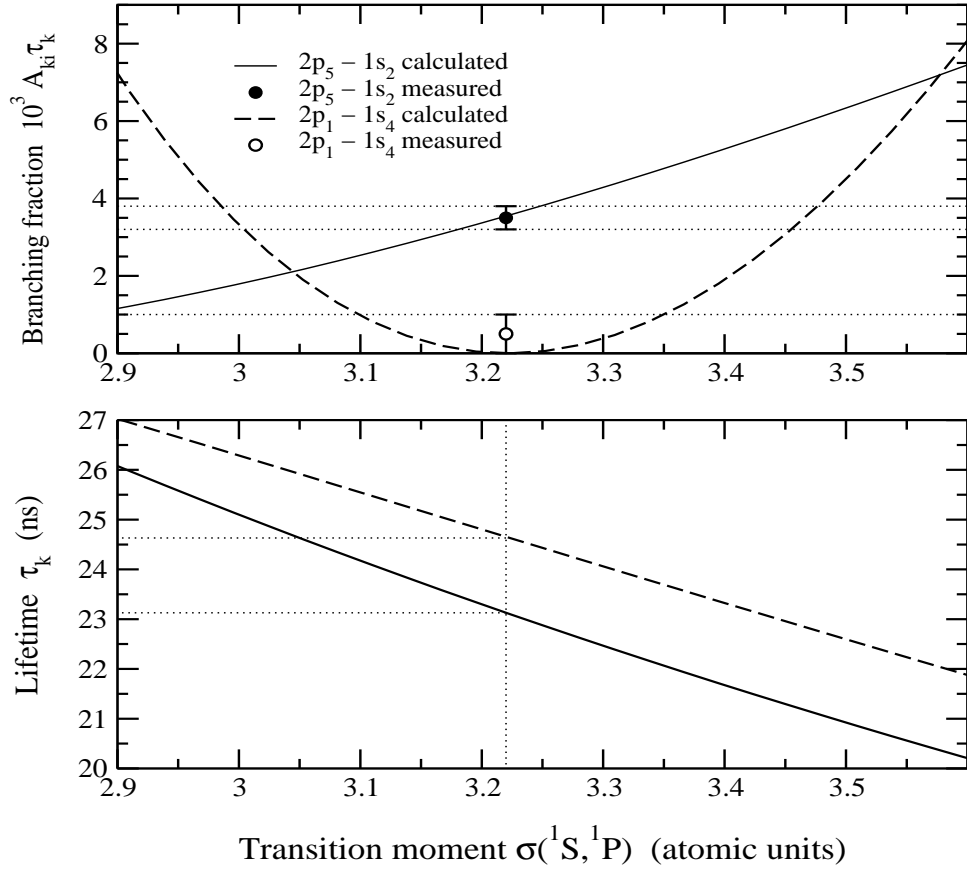


Figure 3: Dependence of lifetimes and branching fractions of the levels $2p_1$ and $2p_5$ on the transition moment $\sigma(^1S, ^1P)$. The top part of the figure shows how the measured branching fraction determines the transition moment which, in turn, determines the lifetime, as illustrated in the bottom part of the figure.

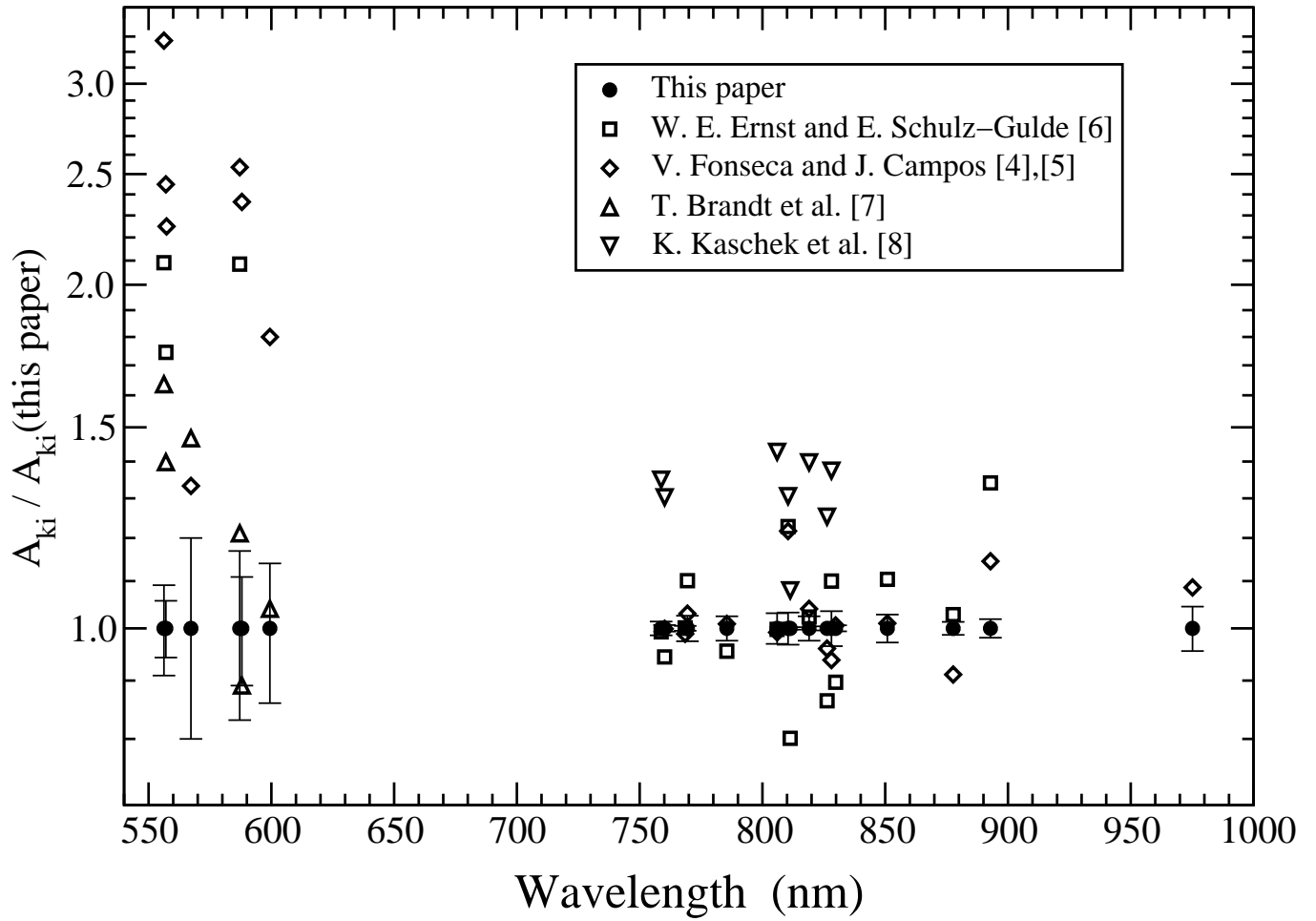


Figure 4: Ratio of transition rates from several earlier experiments and our results.

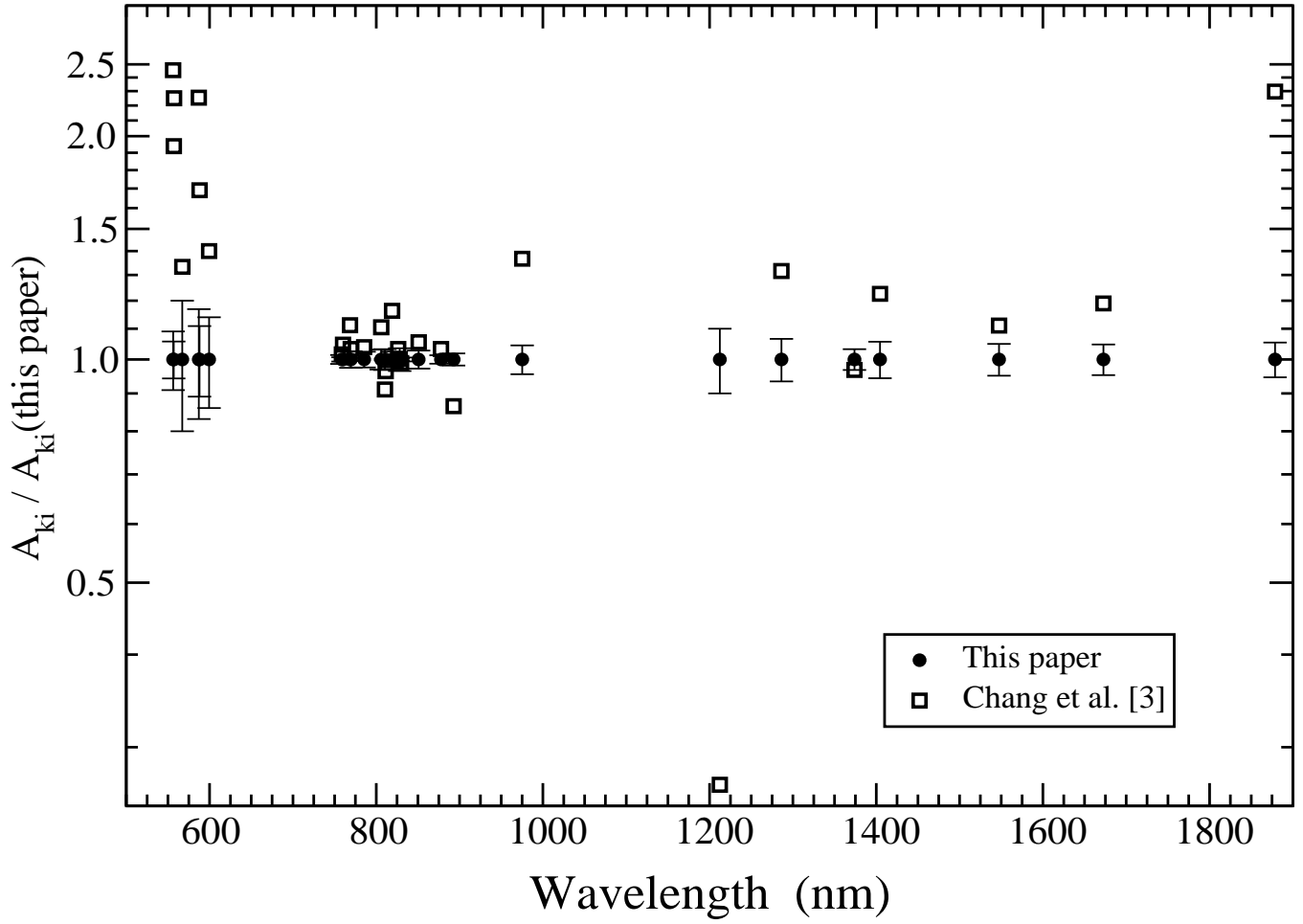


Figure 5: A comparison of our transition rates with the complete set of 5p–5s transition rates measured by Chang, Horiguchi and Setser [3].

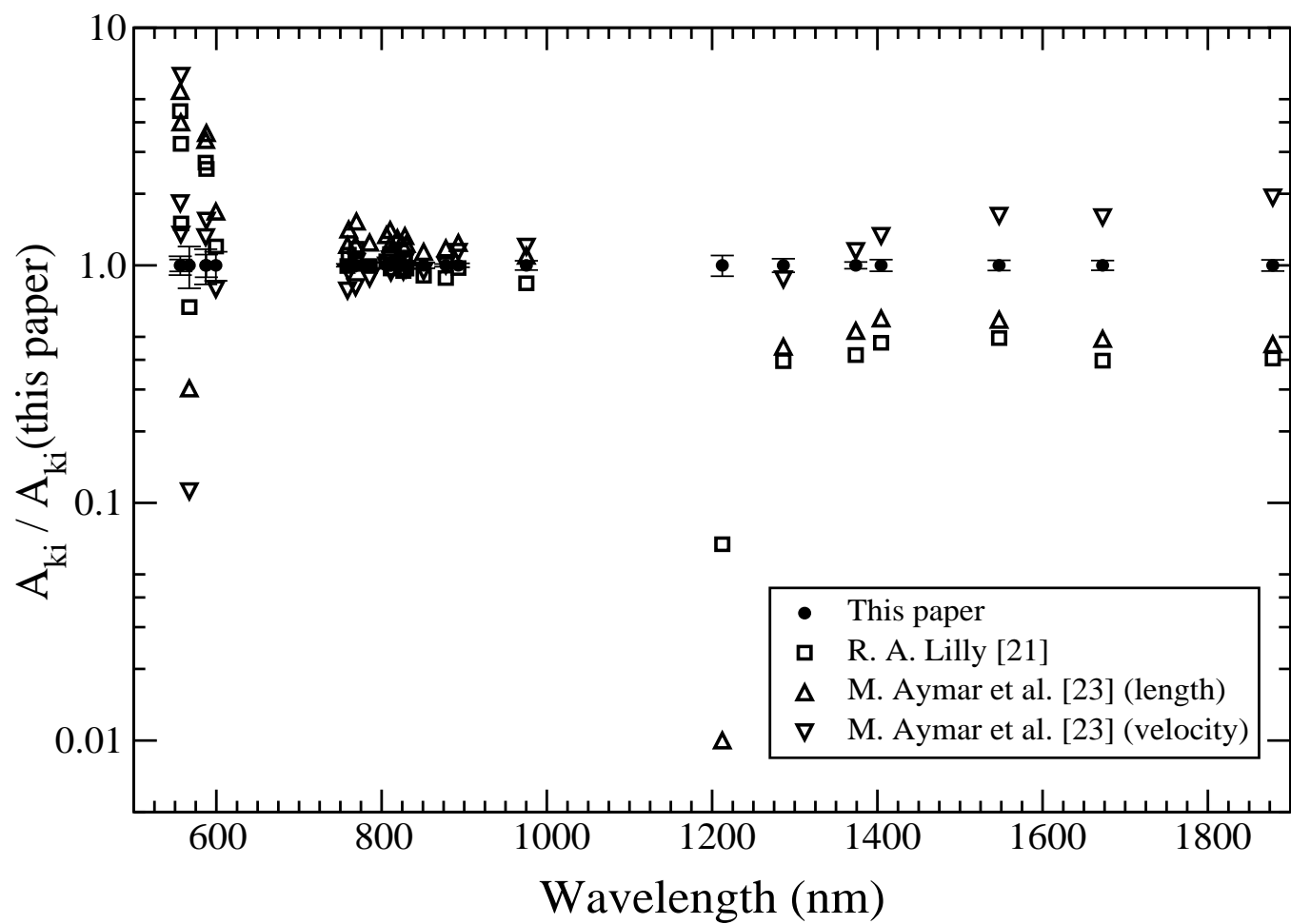


Figure 6: A comparison of our transition rates with theoretical transition rates.